HHS Public Access

Author manuscript

J Opt Soc Am A Opt Image Sci Vis. Author manuscript; available in PMC 2015 June 05.

Published in final edited form as:

J Opt Soc Am A Opt Image Sci Vis. 2014 December 1; 31(12): 2703–2710.

Noise Characterization of Supercontinuum Sources for Low Coherence Interferometry Applications

William J. Brown[1], **Sanghoon Kim**[1], and **Adam Wax**[1,*]

[1]Department of Biomedical Engineering and Fitzpatrick Center for Photonics, Duke University, Durham, North Carolina 27708, USA

Abstract

We examine the noise properties of supercontinuum light sources when used in low coherence interferometry applications. The first application is a multiple-scattering low-coherence interferometry (ms2/LCI) system where high power and long image acquisition times are required to image deep into tissue. For this system we compare the noise characteristics of two supercontinuum sources from different suppliers. Both sources have long term drift that limits the amount of time over which signal averaging is advantageous for reducing noise. The second application is a high resolution optical coherence tomography system where broadband light is needed for high axial resolution. For this system we compare the noise performance of the two supercontinuum sources and a light source based on four superluminescent diodes (SLDs) using imaging contrast as a comparative metric. We find that the NKT SuperK has superior noise performance compared to the Fianium SC-450-4 but neither meets the performance of the SLDs.

1. Introduction

As low coherence interferometry (LCI) has expanded its applications from white light interferometry used to assess lens quality [1] to optical coherence tomography (OCT), used for biomedical imaging [2], the need for broadband light sources with high spectral density has increased. Most commercial OCT systems now use superluminescent diodes (SLDs) which are essentially laser diodes without a cavity. The very high gain of these diodes permits amplified spontaneous emission across the entire wavelength gain range of the diode and since they use manufacturing methods similar to laser diodes, they are relatively inexpensive, with prices ranging from $1,000 up to approximately $20,000 for a fiber coupled version with 160 nm to 190 nm in bandwidth. These broadband SLDs typically consist of multiple diodes which are coupled together [3] either with wavelength coupling or power coupling and are limited to wavelengths where diodes are available.

Previously, the easiest way to provide greater bandwidth from a single device was to use a white light source such as a tungsten lamp. While overall output power could be quite high, the power in a single transverse mode was much lower and this limited their use in LCI [4]. Supercontinuum sources significantly increased the power and wavelength range available

*Corresponding author: a.wax@duke.edu.

in a single transverse mode [5]. Supercontinuum sources use a nonlinear fiber and a high repetition rate laser to generate light with a wavelength range of 400 nm to 2.5 μm . Such sources have been available from NKT Photonics (Birkerød, Denmark) and Fianium (Southampton, United Kingdom) for the last few years and numerous labs have built their own supercontinuum sources [6].

A drawback to supercontinuum sources is the relative intensity noise (RIN) generated by pulse to pulse variation [7, 8]. Particularly for high SNR applications such as OCT, the noise generated by the supercontinuum source has been viewed as a limit to their usability in imaging systems [9, 10].

In this paper we report on the noise characterization of two supercontinuum sources using two low coherence interferometry imaging systems. The first supercontinuum source is a next generation low noise source from NKT Photonics and the second is a current generation supercontinuum source from Fianium.

The first experimental setup is a multiple-scattering low-coherence interferometry (ms2/LCI) system designed and built in our lab [11]. Ms2/LCI is a variation on OCT, but with an imaging range of 8 mm in tissue [12]. A supercontinuum source provides high power across the range of 600 – 670 nm. Additional processing gives spectroscopic contrast. This system is designed to collect long exposures, up to a minute or more, by averaging many acquisitions, which are individually acquired at a rate of 150 per second.

The second system is a commercial Spark OCT system for research from Wasatch Photonics (Durham, North Carolina). This system has an a-scan rate of up to 40 kHz, but by reducing the integration time to 6 μs the noise can be measured at an effective line rate of 160 kHz. In the OCT system, the noise performance of the two supercontinuum sources is also compared to the source with four SLDs from Exalos (Schlieren, Switzerland) that came with the system.

To measure the noise performance, we take a slightly different approach than the previous measurements which introduce a known loss in the sample path and measure a peak height relative to the noise floor [13]. We focus on the noise due to the reference arm light without any sample arm light, thus eliminating any sensitivity to optimization of sample arm coupling back into the LCI system, which can be a drawback to this approach. In the OCT setup, we present OCT images and calculate an image contrast thereby providing a practical metric of the usability of these images independent of the source of the noise. The phantoms used here can easily be replicated allowing others to perform similar measurements and provide a comparison of imaging performance across OCT systems.

2. Experimental Design

Instrument Layout – ms2/LCI system

The ms2/LCI instrument has been described previously [11]; here we give a brief overview. A block diagram of the system is shown in Figure 1(a). Light from a supercontinuum laser is passed through a fiber to filter the light to the range of 600 nm to 700 nm. This light is split

into sample and reference arms. Light in the sample arm is collimated and passed through one side of a lens and is then focused onto the sample at an angle of approximately 4°.

Light returning from the sample is mixed with the reference field and coupled into a single mode fiber for delivery to the spectrometer used for spectral detection. The spectrometer offers 60 nm of bandwidth, with an adjustable center wavelength. An 1800 l/mm grating disperses the collimated output from the fiber, which is then focused onto the camera by an objective lens. The sensor is a 12-bit CCD camera (Dalsa Piranha), 4096 × 96 pixels with a pixel size of 7 × 7 μm and a maximum line rate of 20 kHz. During operation, the vertical direction is fully binned to operate as a line scan camera. The pixel limited spectral resolution is 14.7 pm giving a theoretical imaging range (z_{max}) of 6.8 mm in air [14].

For the noise characterization experiments below, acquired spectra were individually resampled from wavelength onto an axis linearly spaced in wavenumber (k) by interpolation. Final numerical dispersion compensation was performed on each spectrum as described by Zhu et al. [15].

Instrument Layout - OCT system

A schematic of the Spark OCT system is shown in Fig. 1(b). A Michelson interferometer is employed using a 50/50 fiber splitter. The light source for this system is a 4 SLD tower from Exalos with a center wavelength of 840 nm and a 3dB bandwidth of 155 nm. Typical output power at the source is 4 mW coupled into a single mode fiber. The spectrometer is matched to this light source and covers the range of 745 nm to 925 nm with 2048 pixels. The sensor array is from Awaiba (Madeira, Portugal) with pixels that are 7 microns wide and 500 microns tall and can operate at a line rate up to 40 kHz with a digitization depth of 10 bits. For these experiments, the line rates were 10 kHz which has a bit depth of 12, and 20 kHz which has a bit depth of 11. In the sample arm there is a motorized polarization controller with user controlled adjustment. Optical scanning across the sample is accomplished with a MEMS mirror (Mirrorcle, Richmond, CA) with a scan range of 6 mm and a typical spot size of 8 microns.

Supercontinuum Light Sources

We compare the noise characteristics of two supercontinuum light sources. The first is a SC-450-4 from Fianium that is several years old. This source was used in our previously reported work on ms2/LCI [11]. This light source covers the range 460 nm to 2 μm with an average output power of 4 W. It operates at an internal pulse rate of 40 MHz

The second light source is a new supercontinuum model from NKT Photonics, the SuperK Extreme Low Noise, specifically designed for a low noise output. It generates light in the range of 600 nm to 1.75 μm with a total output power of 930 mW across the visible wavelengths and 6 W across the entire spectral range. The internal repetition rate is 78 MHz.

Sensitivity and Noise in LCI

In an LCI scheme, the optical power detected by each channel is the sum of three terms [14]:

$$P(k)=P_R(k)+P_s(k)+\sum_n^N 2\sqrt{P_R(k)P_{sn}(k)}\cos(2k\Delta z_n) \quad (1)$$

for a given wavenumber k, where Δz_n is the location of each reflector n in the sample with a path length difference Δz between the sample and reference interferometer arms. The detected reference and sample powers for each channel are $P_R(k)$ and $P_S(k)$ respectively. These terms are not modulated by the cosine term and thus appear at $z=0$ when the spectral domain signal is Fourier transformed to the spatial domain. The third term is the cross-correlation between the sample and reference arm, and gives rise to the sample's depth reflectivity profile (a-scan).

The signal to noise ratio in LCI is defined as the mean squared signal over noise variance: $SNR=\left\langle S^2\right\rangle/\sigma^2_{noise}$ [13, 14, 16, 17]. Spectral domain LCI detects the real part of the complex spectral density, with the total signal $\langle S^2\rangle$ equal to the number of detected photoelectrons during an acquisition of durationz Δt:

$$\left\langle S^2\right\rangle=(\eta^2\Delta t^2/E_v^2)P_RP_S \quad (2)$$

Here η is the detector quantum efficiency and E_v is the energy of one photon. The noise variance is the sum of several noise sources, including detector receiver noise, composed of both dark noise and read noise, relative intensity noise, and shot noise, $\sigma^2_{noise}=\sigma^2_{read}+\sigma^2_{dark}+\sigma^2_{RIN}+\sigma^2_{shot}$. Read noise is invariant with acquisition parameters and generally depends on specific detector electronics. Dark noise is less than the read noise since the integration times range from 10 ms down to 6 μs. The relative intensity noise (RIN) scales with source power and bandwidth [17]. This term is a significant noise source for supercontinuum sources, unlike SLDs and Ti:Sapphire lasers where it is minimal. Shot noise is described by Poisson statistics with variance given (in units of electrons squared per measurement) by [14]:

$$\sigma^2_{shot}=\eta(P_R+P_S)\Delta t/E_v \quad (3)$$

The design goal of LCI systems is to have the read, dark, and relative intensity noise be lower than the shot noise level, in which case the measurement is described as shot noise limited. In this limit, reference power drops out of the signal to noise ratio (defined here in units of dB):

$$\left\langle S^2\right\rangle/\sigma^2_{shot}=\eta P_S\Delta t/E_v \quad (4)$$

Both the interferometric signal strength and shot noise scale with the square root of the reference power. Thus, sensitivity in the shot noise limit solely depends on the number of sample photons detected. To increase the system OSNR, multiple images can be taken and averaged together as has been previously shown [18, 19]. If other noise sources are present, one will reach a limit where further averaging no longer increases OSNR.

Samples

Samples consisted of two variations of Scotch™ transparent tape. The first sample was six layers of tape on top of card stock, providing a flat sample, and the second was a roll of tape, cut in half giving a curved surface. OCT images of Scotch tape provide a good head to head comparison between OCT systems because there are features that are near the resolution limit of the system and the multiple layers give a depth profile which can be used to assess dynamic range and signal to noise ratio. Since the sample is static and relatively uniform, there is less variation that would be seen in a biological sample. Furthermore, imaging artifacts such as side lobes, due to light source ripple over wavelength or etaloning, due to variation in detector responsivity over wavelength, are also visible.

3. Results

ms2/LCI noise measurements

As noted above, the ms2/LCI system averages several acquisitions to achieve long integration times, up to a minute, in order to reach the very high optical signal to noise ratio (OSNR) levels needed for imaging deep into scattering samples such as tissue. We have previously shown that this system can reach OSNR levels of 140 dB, which combined with our multiscattering technique allows imaging up to 1 cm into tissue [12]. This technique is critically dependent on the increase in OSNR that comes with averaging multiple a-scans and thus it is important to know what the limits are to averaging with supercontinuum sources.

The ms2/LCI system was operated with a line rate of 150 a-scans per second with averaged sets of a-scans ranging from a single a-scan up to 30,000 a-scans. Since the system does not have the capability to store more than a few hundred a-scans, larger sets were averaged into groups of 10, 100, and 1,000 a-scans before being saved. All averaging was performed after the amplitude of the Fast Fourier Transform (FFT) was calculated. Multiple sets of data were taken for each number of averages so that statistical measurements across a-scans could be performed. The target was to combine at least 50 acquisitions for each degree of averaging.

Looking first at the data from the NKT SuperK, Figure 2(a) shows the FFT for 100 a-scans where each a-scan is an average of 10 acquisitions. In this figure the x-axis is imaging depth, which is maximum of 6.8 mm for this system, the z-axis is 100 different a-scans, and the y-axis is noise level in arbitrary units. Note that there is significant structure in the noise, primarily for the imaging depth range of 0 to 2 mm. By measuring the noise level as the standard deviation within an a-scan, and then averaging across a-scans, we generate Figure 2(c). The four curves correspond to measurements of the noise across the entire imaging range of 0 to 6.8 mm, as well as smaller ranges of 1.7 mm to 6.8mm, 3.4 mm to 6.8 mm and 5.1 to 6.8 mm. In all cases the increase in OSNR saturates after a certain number of averages; for the full range there is only about 1 dB of improvement, but for the deepest imaging range (5.1 to 6.8 mm) the improvement is ~17 dB. This result is somewhat similar to a characterization shown in our previous work [11], but there the saturation level was even higher since smaller depth ranges of ~0.5 mm were used for measuring the noise. The

structural nature of the noise means that once averaging reduces the other sources of noise to the same level as the underlying slope or structure of the noise, additional averaging has no effect, i.e. OSNR will not improve further.

In order to facilitate comparisons, we select a metric consisting of the ratio of the area under curve of OSNR improvement versus number of averages compared to the straight line at 45 degrees which represents ideal averaging. This metric (which we will refer to as OE for OSNR enhancement) ranges from 0, where there is no OSNR increase with averaging, up to 1.0, where averaging increases the OSNR along the ideal curve, i.e. as the square root of the number of averages. For Figure 2(c) the OE ranges from 0.01 for the full imaging ranges up to 0.56 for the imaging range of 5.1 to 6.8 mm.

To reduce the effect of the underlying structure in the noise, we took a long time average of 10,000 a-scans and then subtracted this from other a-scans before calculating the averages. Figure 2(b) shows the data from 2(a) with the long term average subtracted out. There is still some depth dependence to the noise features with larger noise amplitude near DC, but it is significantly less than that shown in Figure 2(a). The OSNR increase as a function of averaging for the background subtracted data is shown in Figure 2(d) where we see that for the full imaging range of 0 to 6.8 mm the OSNR advantage increases from ~1dB up to ~26 dB, giving an OE of 0.78. The bottom quarter, 5.1 to 6.8 mm increases from ~17 dB to ~37 dB, with an OE of 0.93.

An alternate way to measure the noise is by looking at statistical variation across multiple a-scans instead of within an individual a-scan. This approach is naturally insensitive to any underlying structure of the noise and only measures the variations across time. Figure 2(e) shows the OSNR improvement based for this approach. For the full imaging range the improvement reaches ~37 dB before actually rolling over and decreasing for additional averaging. This roll over effect slightly decreases the OE, resulting in a value of 0.91. For the three deeper subsections the OSNR improvement reaches ~41 dB with an OE average of 0.98.

The OSNR improvement curves in Figure 2(d) and 2(e), while not identical, are within 5 dB of each other particularly for the imaging ranges that do not include the section closest to DC. This is to be expected, subtracting out a long term average and looking at the noise within a-scans should be similar to the noise across multiple a-scans.

The other feature to note is the roll over in the OSNR improvement once a certain number of averages is reached. This suggests that there is another source of variation that occurs on these longer time scales. For this system running at 150 Hz, the maximum OSNR increase occurs between 3,000 and 7,000 scans, corresponding to total signal collection times of 20 to 50 seconds. This trend appears in the OE value data which will reach a point where it starts to drop below 1 for increasing number of averages. Possible sources of this variation include thermal effects and the time constant present for feedback loops in the supercontinuum laser. For the ms2/LCI system, this time is important to know since it sets the limit of the overall system OSNR and the maximum time for averaging that may be used while imaging a single point.

These noise measurements and analysis were repeated using the Fianium supercontinuum with the results shown in Figure 3. The raw a-scans are shown in Figure 3(a) where again each a-scan is the average of 10 acquisitions. Figure 3(b) shows the OSNR improvement when the noise is calculated by analyzing the variation between successive a-scans with the given number of averages. The full range OE is 0.90 and the deeper ranges reach 0.99.

The results for the Fianium unit are quite similar to the NKT unit. There is slightly more noise around DC for the Fianium unit, see left side of Figure 3(a) compared to Figure 2(a), but it has minimal impact on the OSNR improvements with averaging. This is probably not surprising, since each averaged acquisition consists of a massive number of pulses from the source. The NKT is pulsing at 78 MHz, so 1 minute of signal acquisition corresponds to 4.68×10^9 pulses and the Fianium running at 40 MHz generates 2.40×10^9 pulses in the same time interval. Since both the NKT and Fianium exhibit the roll-over behavior for longer signal acquisition times, it would be worth further investigation to understand if that variation is coming from effects within the sources or variations in the rest of the system.

OCT noise measurements

In contrast to the ms2/LCI system where long integration times are needed, the goal of OCT systems is to image quickly, both to generate as much imaging information as possible and to minimize the impact of the movement of biological samples. In the configuration used, the Spark system has a maximum line rate of 20 kHz which corresponds to an integration time of 44 μs per a-scan. However the integration time can be set independent of the line rate and so noise levels were measured down to a minimum integration time of 6 μs .

To measure the impact of light source noise in the OCT system, we first measured the noise level due to light from only the reference arm, with no light in the sample arm, see Figure 4. Standard OCT imaging processing is performed, including subtracting a background level comprised of 1,000 a-scans averaged together. This removes the fixed pattern noise from the CMOS line scan array in the spectrometer. Noise levels are shown for three integration times, with Figures 4(a), 4(b) and 4(c) corresponding to integration times of 94, 24, and 6 μs respectively. At each integration time and light source the power in the reference arm is adjusted so that the level reaches the target of 75% of the full well depth of the line scan array. For the 94 μs integration time, the line acquisition time for the camera is 97 μs , or approximately 10,000 a-scans per second, and for all other integration times the line acquisition time is 47 μs or approximately 20,000 a-scans per second. In all plots the thick green line is the noise level for the Fianium, the medium blue line is for the NKT SuperK, and the thin red line is for Exalos SLD tower.

For 94 μs integration time the NKT noise level is approximately 15 dB above the SLD noise level at the left side of the curve (which corresponds to DC in the FFT or the topmost pixel of the OCT image) but falls to near the level of the SLD by ~1 mm of imaging depth. The Fianium noise level is ~25 dB above the SLD noise level at 0 mm, but again is very close to the SLD noise level by 1 mm imaging depth. Since the optical power at the spectrometer is the same for each light source, the excess noise above the SLD level is primarily RIN in the supercontinuum sources.

As the integration time is shortened to 24, and 6 μs, the SLD noise level appears to fall – this is because for this integration time the SLD does not have sufficient optical power to reach the 75% fill level on the spectrometer sensor. The supercontinuum sources have significantly more power and can fill the spectrometer sensor's wells all the way down to the 6 μs integration time. For the shorter integration times the noise level near 0 mm continues to increase for both supercontinuum sources, but from 1 to 2 mm remains within a few dB of the noise level from the 44 μs integration time in Figure 4(c). In terms of the number of supercontinuum pulses, at 96 μs the NKT SuperK is generating 7,500 pulses and the Fianium SC-450-4 is generating 3,840 pulses while at 6 μs the pulse counts are 468 and 240 respectively.

The NKT SuperK noise level is consistently 10 dB lower than that of the Fianium, which suggests significant improvement in the RIN of this SuperK source. However, since the goal is shot noise limited performance, there is still opportunity for further improvement, but this light source is much more acceptable for OCT imaging then previous units.

OCT imaging

To further elucidate the effects of the supercontinuum noise levels, we imaged a phantom made of six layers of Scotch tape on top of a business card. This phantom allows simultaneous assessment of the resolution of the system by looking at each tape layer, the optical power by looking at the imaging depth within the card stock underneath the tape, and the contrast by comparing dark and light signal levels between the tape layers. Figure 5 shows the same phantom imaged with the three different light sources with the Exalos SLD on the left, the NKT SuperK in the middle and the Fianium on the right. Each image consists of an average of 50 b-scans and the integration time for each a-scan is 44 μs. In the lower right of each b-scan image is an inset of an a-scan from the middle of that image.

To provide a metric for comparison across the images, we calculate the contrast using the signal strength difference between the top and bottom of the top layer of tape. Using the Michelson contrast definition (relative contrast = $(I_{max} - I_{min}) / (I_{max} + I_{min})$) the maximum contrast for the SLD image is 0.54, for the NKT is 0.43 and for the Fianium is 0.27. This is consistent with the visual interpretation of the images. The images from the supercontinuum sources have higher signal levels at the top of the tape and image deeper into the paper underneath the tape. This is due to the higher optical power available at the sample, with the NKT providing 7.9 mW, the Fianium providing 8.9 mW, and 1 mW from the Exalos SLD. Power levels in the sample arm are optimized for maximum power at the sample.

Note that the intensity is on a logarithmic scale, resulting in a change to the relative contrast which is typically used with linear scaling. However this is a reasonable approach since the full dynamic range of an OCT image can be up to 100 dB, but the local contrast is rarely more than 30 dB. Using relative contrast on a tape phantom may provide a way to compare OCT system performance of different systems and at different times since the phantom is easy to acquire and the relative contrast calculation as used here reduces the impact of the variability in imaging processing approaches.

OCT imaging with EDI

Since the additional noise seen in the supercontinuum images is primarily RIN, it is possible to minimize the noise impact by moving the imaging area away from DC (0 mm) in the FFT. One approach to implement this is enhanced depth imaging (EDI), which is a technique that has been previously used to balance the fall-off in SD-OCT spectrometers [20] against the signal attenuation within samples. In this case EDI will move the sample away from the higher noise part of the a-scan. EDI is implemented by increasing the length of the reference arm in the OCT system so that the image wraps around the zero point and moves to the opposite side of DC, into the complex conjugate portion of the FFT. It now appears upside down in the image window in the OCT software. It is typically necessary to modify the dispersion compensation values when using EDI, which we did to re-optimize the image.

Figure 6 shows OCT images of a roll of tape using EDI. As in Figure 5, the image using the Exalos SLD is on the left, the image using the NKT is in the middle and the image from the Fianium is on the right. These images have been reflected about the horizontal midpoint so that the top of the sample is still the top of the image. Thus the DC point of the FFT is now at the bottom of the OCT images. Inset in each OCT image is an a-scan from the middle of the b-scan; note that in these graphs the DC of the FFT is still on the left side and the maximum imaging depth is on the right side. Using the same method for measuring the contrast for the top layer of tape we now find the SLD relative contrast is 0.71, for the NKT it is 0.63, and the Fianium is 0.59.

The overall signal improvement in EDI mode is limited by the fall-off in the spectrometer, which for the Spark system is ~25 dB at the full imaging depth. The relative contrast is independent of the spectrometer fall-off so increases are at least partially due to the lower RIN at the deeper imaging depths. Improving the spectrometer fall-off will improve the overall signal level of the images in EDI mode.

4. Discussion

We have measured the noise levels of broadband light sources in two low coherence interferometry systems. The ms2/LCI system provides a platform for long time measurements up to a minute while the OCT system provides data with an integration time as short as 6 μs. This gives a range of number of optical pulses from the supercontinuum sources averaged into a single acquisition of 4 billion down to 240. We looked at noise levels from a typical supercontinuum source from Fianium and well as a new model from NKT that is specifically designed to have lower noise levels.

In the ms2/LCI system we measure the noise spectrum and provide FFT's of the spectrum. The increase in OSNR is measured as a function of averaging and we note the differences in OSNR improvement for noise calculated within an a-scan versus noise measured across a-scans. This difference appears to be due to the frequency dependence of the noise which is consistent with RIN. We find that the OSNR continues to increase up to total acquisition times of 20 to 50 seconds and then decreases for further averaging. We define OE and use it as a metric to quantify the system performance and note that the OE increases for deeper

imaging ranges, suggesting a frequency dependence to the RIN. The OE is sufficient for the ms2/LCI system to reach overall OSNR levels of 140 dB, indicating that either supercontinuum source is fit for the purpose of this system.

In the OCT system we measure the average noise levels as a function of integration time and note the need to subtract out the fixed pattern noise in the CMOS line scan array used in the spectrometer. OCT images of a phantom consisting of tape on a card show a reduction in relative contrast for the supercontinuum sources compared to the SLD. The NKT supercontinuum shows better relative contrast than the Fianium unit, but still not as good as that seen for the SLD source.

One way to mitigate the noise effects in the supercontinuum sources is to use EDI to move the image away from the high noise levels near DC. We show sample images of a roll of tape and measure the increased relative contrast. All sources show improved relative contrast, but the improvement of the supercontinuum sources put them within 11% of the SLD for the NKT and 27% for the Fianium. This method will be even more useful in systems with less spectrometer fall-off than that used here.

Conclusion

Supercontinuum light sources have shown tremendous improvement and are now viable options for low coherence interferometry systems. The combination of high power and very broad bandwidth in a single mode provide functionality that is unavailable in any other light source. New supercontinuum sources such as the NKT SuperK Low Noise, have better noise performance compared to older designs such as the Fianium SC-450-4. There is still excess RIN compared to the SLD light source, but the supercontinuum noise level is low enough that the trade-off for increased optical power and bandwidth is worthwhile for overall system performance. Use of imaging techniques such as EDI improves contrast and overall system performance.

Acknowledgements

Special thanks to Husain Imam and the NKT Photonics team for the loan of the SuperK low noise supercontinuum laser.

Additional thanks to Michael Crose for technical assistance with the supercontinuum lasers.

We gratefully acknowledge funding support from the National Science Foundation (CBET 1133222), the National Institute of Health (1R21EY023451), and an Innovative Ophthalmic Research award from Research to Prevent Blindness.

References

1. Wyant JC. White light interferometry. 2002:98–107.
2. Izatt JA, Kulkarni MD, Kobayashi K, Barton JK, Welch AJ. Optical coherence tomography for biodiagnostics. Opt. & Phot. News. 1997; 8:41–47. 65.
3. Ko T, Adler D, Fujimoto J, Mamedov D, Prokhorov V, Shidlovski V, Yakubovich S. Ultrahigh resolution optical coherence tomography imaging with a broadband superluminescent diode light source. Optics Express. 2004; 12:2112–2119. [PubMed: 19475046]

4. Graf RN, Brown WJ, Wax A. Parallel frequency-domain optical coherence tomography scatter-mode imaging of the hamster cheek pouch using a thermal light source. Opt. Lett. 2008; 33:1285–1287. [PubMed: 18552933]
5. Wadsworth WJ, Ortigosa-Blanch A, Knight JC, Birks TA, Man T-PM, Russell PSJ. Supercontinuum generation in photonic crystal fibers and optical fiber tapers: a novel light source. JOSA B. 2002; 19:2148–2155.
6. Povazay B, Bizheva K, Unterhuber A, Hermann B, Sattmann H, Fercher AF, Drexler W, Apolonski A, Wadsworth WJ, Knight JC, Russell PSJ, Vetterlein M, Scherzer E. Submicrometer axial resolution optical coherence tomography. Opt. Lett. 2002; 27:1800–1802. [PubMed: 18033368]
7. Corwin K, Newbury NR, Dudley J, Coen S, Diddams S, Weber K, Windeler R. Fundamental noise limitations to supercontinuum generation in microstructure fiber. Phys. Rev. Lett. 2003; 90:113904. [PubMed: 12688929]
8. Møller U, Sørensen ST, Jakobsen C, Johansen J, Moselund PM, Thomsen CL, Bang O. Power dependence of supercontinuum noise in uniform and tapered PCFs. Opt. Express. 2012; 20:2851–2857. [PubMed: 22330522]
9. Froehly L, Meteau J. Supercontinuum sources in optical coherence tomography: A state of the art and the application to scan-free time domain correlation techniques and depth dependant dispersion compensation. Optical Fiber Technology. 2012; 18:411–419.
10. Szkulmowski M, Wojtkowski M, Bajraszewski T, Gorczyńska I, Targowski P, Wasilewski W, Kowalczyk A, Radzewicz C. Quality improvement for high resolution in vivo images by spectral domain optical coherence tomography with supercontinuum source. Optics Communications. 2005; 246:569–578.
11. Matthews TE, Giacomelli MG, Brown WJ, Wax A. Fourier domain multispectral multiple scattering low coherence interferometry. Appl. Optics. 2013; 52:8220–8228.
12. Matthews, Thomas; Medina, Manuel; Maher, Jason R.; Levinson, Howard; Brown, William J.; Wax, Adam. Deep spectroscopic tissue imaging with scattered light. Optica. 2014; 1:105.
13. Choma M, Sarunic M, Yang C, Izatt J. Sensitivity advantage of swept source and Fourier domain optical coherence tomography. Optics express. 2003; 11:2183–2192. [PubMed: 19466106]
14. Leitgeb R, Hitzenberger C, Fercher A. Performance of fourier domain vs. time domain optical coherence tomography. Opt. Express. 2003; 11:889–894. [PubMed: 19461802]
15. Zhu Y, Terry NG, Woosley JT, Shaheen NJ, Wax A. Design and validation of an angle-resolved low-coherence interferometry fiber probe for in vivo clinical measurements of depth-resolved nuclear morphology. Journal of biomedical optics. 2011; 16:011003–011003. [PubMed: 21280890]
16. Rollins AM, Izatt JA. Optimal interferometer designs for optical coherence tomography. Opt. Lett. 1999; 24:1484–1486. [PubMed: 18079840]
17. de Boer JF, Cense B, Park BH, Pierce MC, Tearney GJ, Bouma BE. Improved signal-to-noise ratio in spectral-domain compared with time-domain optical coherence tomography. Opt. Lett. 2003; 28:2067–2069. [PubMed: 14587817]
18. Peter HT, Ruikang KW. Digital phase stabilization to improve detection sensitivity for optical coherence tomography. Measurement Science and Technology. 2007; 18:3365.
19. Szkulmowski M, Wojtkowski M. Averaging techniques for OCT imaging. Optics Express. 2013; 21:9757–9773. [PubMed: 23609683]
20. Spaide RF, Koizumi H, Pozonni MC. Enhanced depth imaging spectral-domain optical coherence tomography. American journal of ophthalmology. 2008; 146:496–500. [PubMed: 18639219]

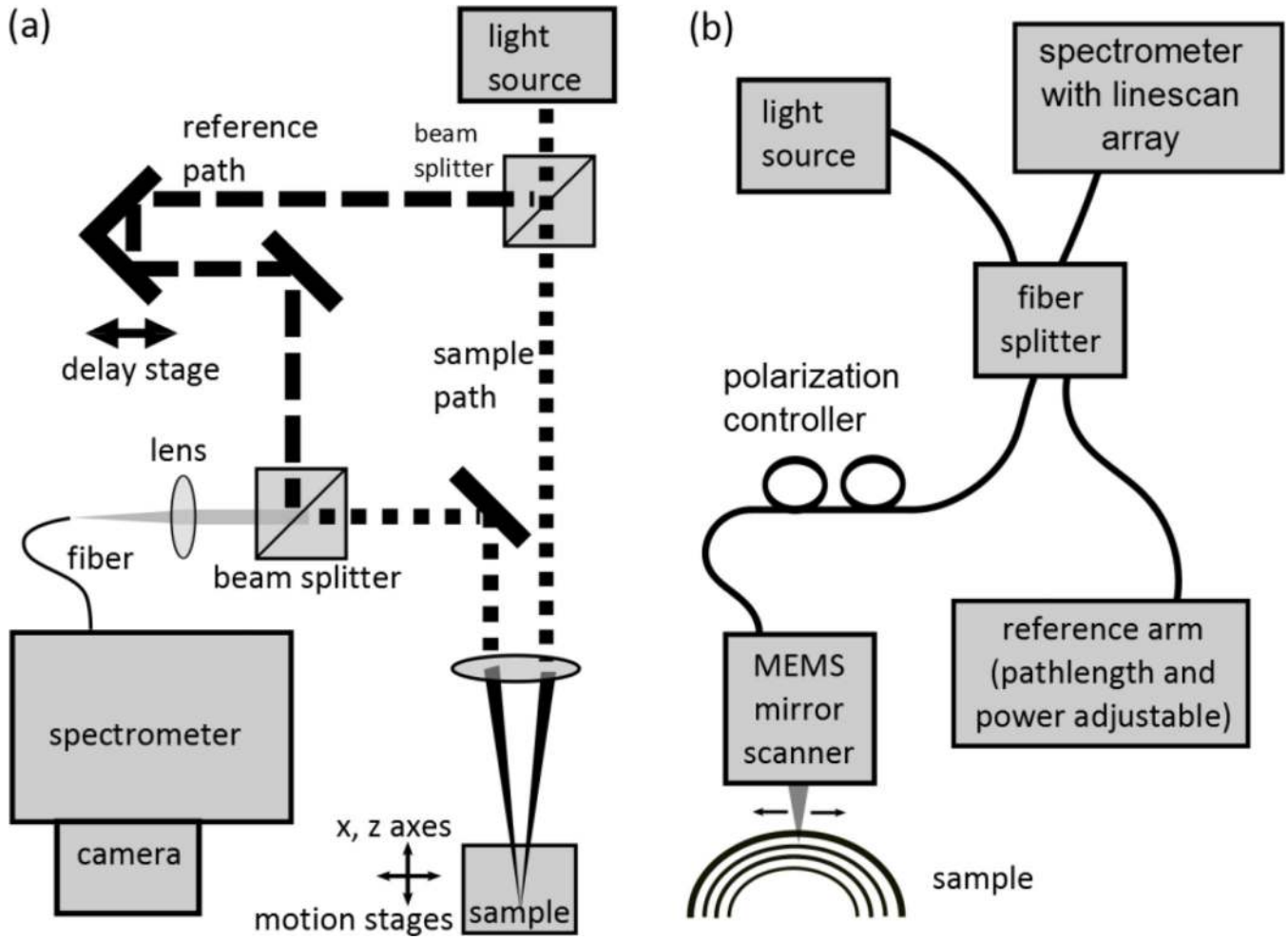

Figure 1.

(a) Diagram of system setup for ms2/LCI system [11]. The ms2/LCI instrument consists of a modified Mach-Zehnder interferometer and a custom spectrometer. The optical path illuminates the sample through one side of a lens and collects multiply scattered light through the opposite side of the same lens, (b) Diagram of system setup for OCT system. System uses a Michelson interferometer with light source and spectrometer on one side of a fiber splitter and sample and reference arms on the other side.

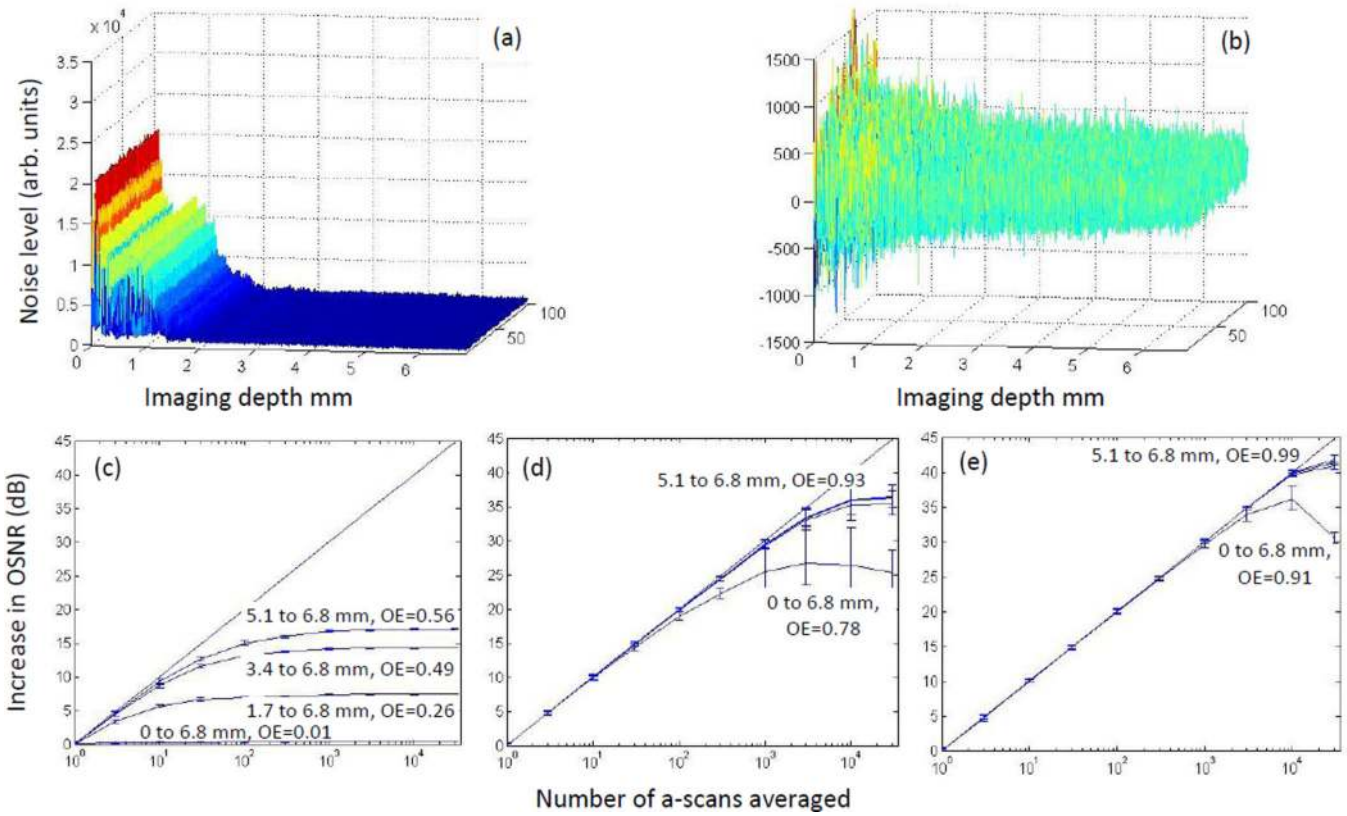

Figure 2.

Noise data and averaging effects for NKT SuperK (a) FFT of noise for 100 a-scans where each a-scan consists of an average of 10 acquisitions and has an imaging depth of 6.8 mm, (b) FFT of the same noise with a long time average background subtracted out, (c) improvement in OSNR as a function of the number of a-scans acquisitions averaged together for 1 to 30,000 acquisitions. Noise is measured within an individual a-scan. Bottom curve is for the full imaging depth of 0 to 6.8 mm, next curve is the range 1.7 to 6.8 mm, next curve is 3.4 to 6.8mm and top curve is 5.1 to 6.8mm, (d) improvement in OSNR as a function of averaging when the noise is calculated within individual a-scans, but a long time average is first subtracted out, and (e) improvement in OSNR as a function of averaging when the noise is calculated across multiple a-scans. For (c), (d), and (e) the straight line represents the ideal case where OSNR increases as the square root of the number of averaged acquisitions.

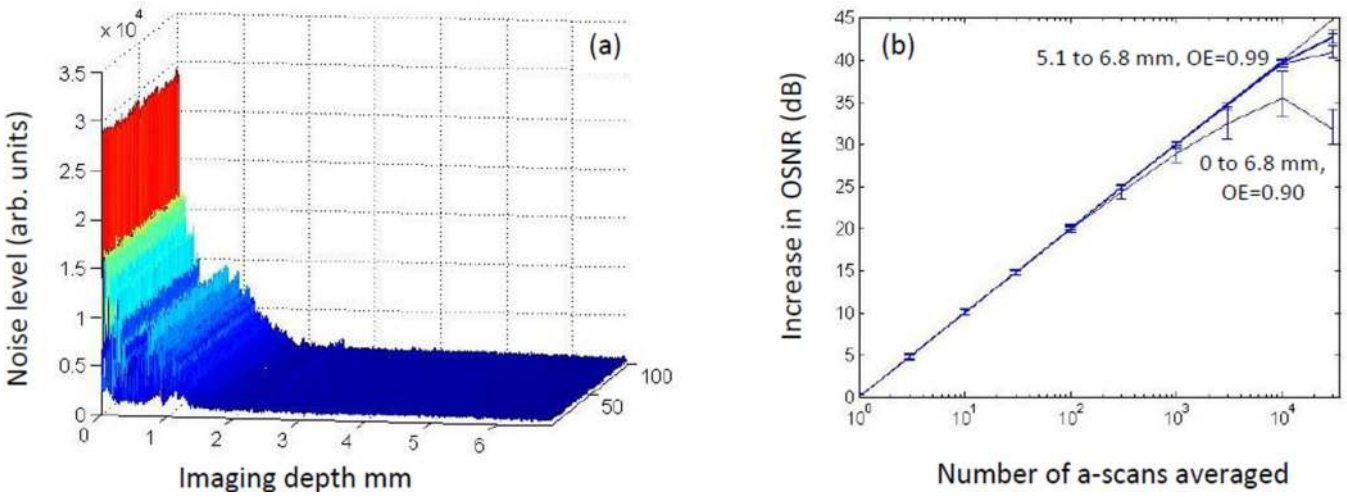

Figure 3.

Noise data and averaging effects for Fianium SC-450-4 (a) FFT of noise for 100 a-scans where each a-scan consists of an average of 10 acquisitions and imaging depth of spectrometer is 6.8 mm, and (b) improvement in OSNR as a function of the number of a-scans acquisitions averaged together for 1 to 30,000 acquisitions where the noise is calculated across multiple a-scans. For (b) the straight line represents the ideal case where OSNR increases as the square root of the number of averaged acquisitions.

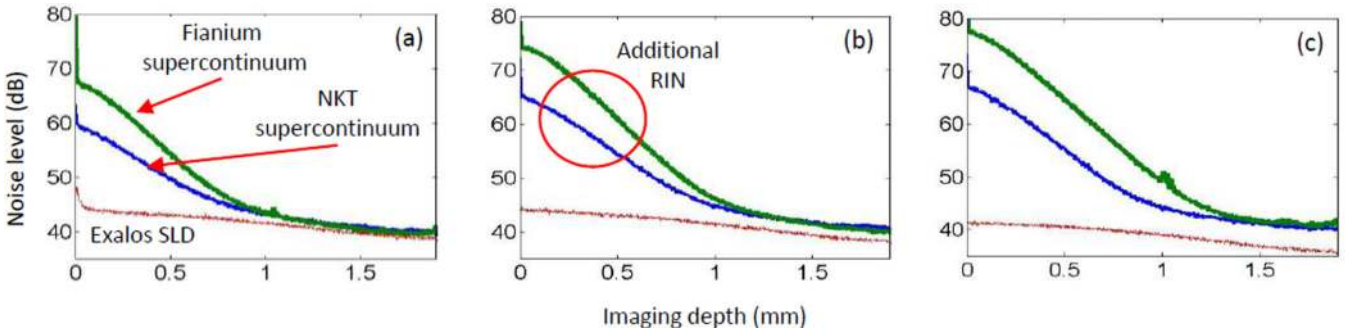

Figure 4.

Noise performance as a function of integration time for the Spark OCT system. (a) Noise from different light sources with 94 μs integration time: thick green curve is Fianium SC-450-4, medium width blue curve is NKT SuperK, and thin red line is SLD, (b) integration time is 24 μs, curve thicknesses and colors are the same as in (a), and (c) integration time is 6 μs .

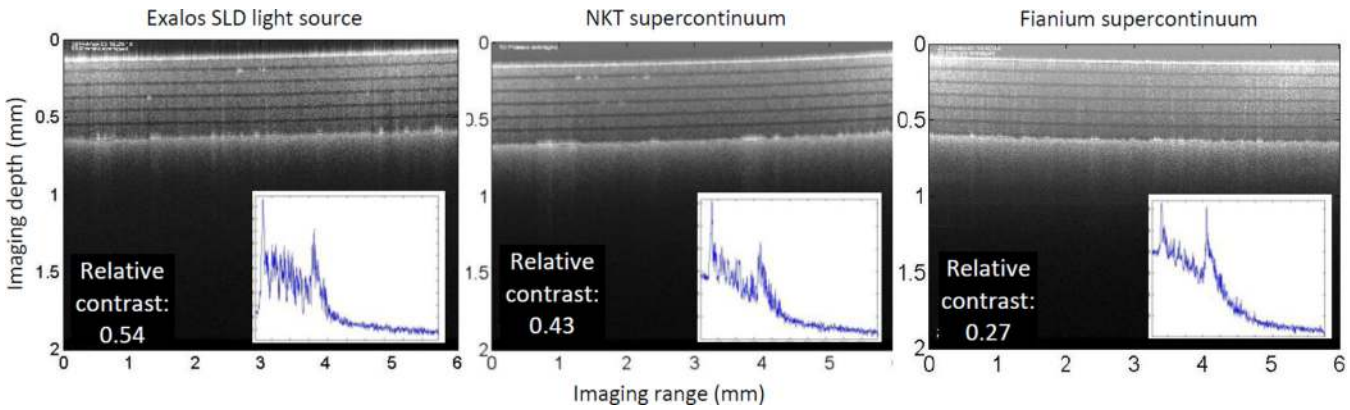

Figure 5.

Images of phantom using Spark OCT with three different light sources. Phantom consists of card stock with 6 layers of tape on top. (a) Light source is Exalos 4 SLD, (b) light source is NKT SuperK, and (c) light source is Fianium SC-450-4. An a-scan from the middle of each image is shown in the inset images. Relative contrast is measured with I_{max} at the top of the first layer of tape and I_{min} at the bottom of the first layer of tape and calculated by relative contrast = $(I_{max} - I_{min})/(I_{max} + I_{min})$.

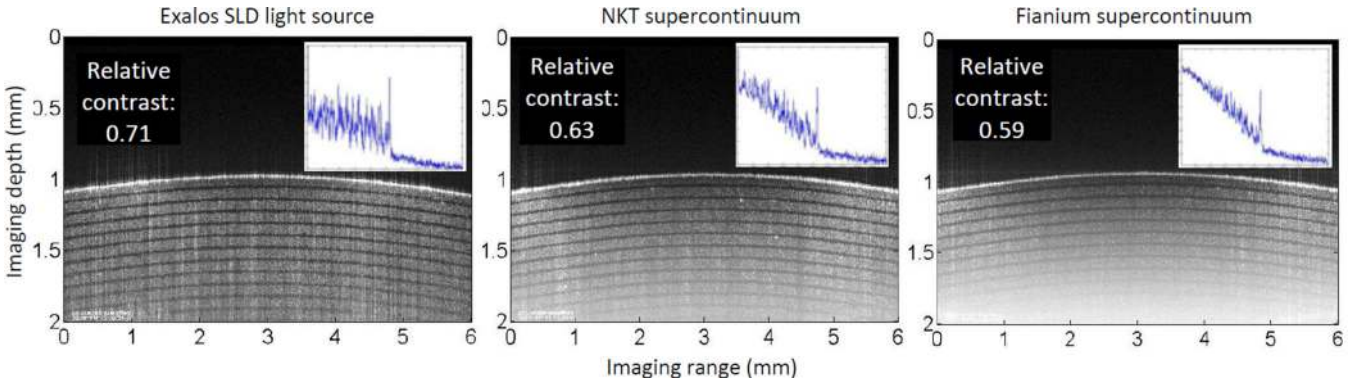

Figure 6.

Enhanced depth imaging (EDI) of a roll of tape using Spark OCT with three different light sources. (a) Light source is Exalos 4 SLD, (b) light source is NKT SuperK, and (c) light source is Fianium SC-450-4. Inset graph is an a-scan from the middle of each image. Relative contrast is measured at the top and bottom of the top layer of tape. EDI mode significantly improves relative contrast for all systems, but more so for the supercontinuum sources.

Table 1

OE values as a function of imaging depth for both light sources and various methods for measuring noise. OE represents the improvement of signal due to averaging as compared to the ideal case. Figure 2 shows graphic representations of a few of these measurements. Noise measurement methods are: (1) noise measured within an a a-scan, (2) noise measured within an a a-scan with a 10,000 acquisition average subtracted out, and (3) noise measured across multiple a-scans.

OE Values	NKT light source			Fianium light source		
Imaging Range (mm)	(1)	(2)	(3)	(1)	(2)	(3)
0 – 6.8	0.01	0.78	0.91	0.03	0.81	0.90
1.7–6.8	0.26	0.92	0.98	0.34	0.92	0.98
3.4–6.8	0.49	0.93	0.99	0.45	0.94	0.99
5.1–6.8	0.56	0.93	0.99	0.55	0.94	0.99